Nonadiabatic vibrational dynamics in the HCO_2^- H_2O complex

Hamm, Peter ; Stock, Gerhard

Abstract: Based on extensive ab initio calculations and the time-propagation of the nuclear Schrödinger equation, we study the vibrational relaxation dynamics and resulting spectral signatures of the OH stretch vibration of a hydrogen-bonded complex, HCO_2^- H_2O. Despite their smallness, it has been shown experimentally by Johnson and coworkers that the gas-phase infrared spectra of these types of complexes exhibit much of the complexity commonly observed for hydrogen-bonded systems. That is, the OH stretch band exhibits a significant red shift together with an extreme broadening and a pronounced substructure, which reflects its very strong anharmonicity. Employing an adiabatic separation of time scales between the three intramolecular high-frequency modes of the water molecule and the three most important intermolecular low-frequency modes of the complex, we calculate potential energy surfaces (PESs) of the ground and the first excited states of the high-frequency modes and identify a vibrational conical intersection between the PESs of the OH stretch fundamental and the HOH bend overtone. By performing a time-dependent propagation of the resulting system, we show that the conical intersection affects a coherent population transfer between the two states, the first step of which being ultrafast (60 fs) and irreversible. The subsequent relaxation of vibrational energy into the HOH bend and ground state occurs incoherently but also quite fast (1 ps), although the corresponding PESs are well separated in energy. Owing to the smaller effective mass difference between light and heavy degrees of freedom, the adiabatic ansatz is consequently less significant for vibrations than in the electronic case. Based on the model, we consider several approximations to calculate the measured Ar-tag action spectrum of HCO_2^- H_2O and achieve semiquantitative agreement with the experiment.

DOI: https://doi.org/10.1063/1.4932189

AIP | The Journal of Chemical Physics

Nonadiabatic vibrational dynamics in the HCO 2 − · H 2 O complex

Peter Hamm and Gerhard Stock

Citation: The Journal of Chemical Physics **143**, 134308 (2015); doi: 10.1063/1.4932189
View online: http://dx.doi.org/10.1063/1.4932189
View Table of Contents: http://scitation.aip.org/content/aip/journal/jcp/143/13?ver=pdfcov
Published by the AIP Publishing

Nonadiabatic vibrational dynamics in the $HCO_2^- \cdot H_2O$ complex

Peter Hamm[1] and Gerhard Stock[2]
[1]*Department of Chemistry, University of Zurich, Zurich, Switzerland*
[2]*Biomolecular Dynamics, Institute of Physics, Albert Ludwigs University, 79104 Freiburg, Germany*

(Received 17 August 2015; accepted 14 September 2015; published online 7 October 2015)

Based on extensive *ab initio* calculations and the time-propagation of the nuclear Schrödinger equation, we study the vibrational relaxation dynamics and resulting spectral signatures of the OH stretch vibration of a hydrogen-bonded complex, $HCO_2^- \cdot H_2O$. Despite their smallness, it has been shown experimentally by Johnson and coworkers that the gas-phase infrared spectra of these types of complexes exhibit much of the complexity commonly observed for hydrogen-bonded systems. That is, the OH stretch band exhibits a significant red shift together with an extreme broadening and a pronounced substructure, which reflects its very strong anharmonicity. Employing an adiabatic separation of time scales between the three intramolecular high-frequency modes of the water molecule and the three most important intermolecular low-frequency modes of the complex, we calculate potential energy surfaces (PESs) of the ground and the first excited states of the high-frequency modes and identify a vibrational conical intersection between the PESs of the OH stretch fundamental and the HOH bend overtone. By performing a time-dependent propagation of the resulting system, we show that the conical intersection affects a coherent population transfer between the two states, the first step of which being ultrafast (60 fs) and irreversible. The subsequent relaxation of vibrational energy into the HOH bend and ground state occurs incoherently but also quite fast (1 ps), although the corresponding PESs are well separated in energy. Owing to the smaller effective mass difference between light and heavy degrees of freedom, the adiabatic ansatz is consequently less significant for vibrations than in the electronic case. Based on the model, we consider several approximations to calculate the measured Ar-tag action spectrum of $HCO_2^- \cdot H_2O$ and achieve semiquantitative agreement with the experiment. © *2015 AIP Publishing LLC.* [http://dx.doi.org/10.1063/1.4932189]

I. INTRODUCTION

The hydrogen bond is a weak chemical bond that is of eminent importance, in particular for biomolecular systems.[1,2] Also, the many anomalies in the thermodynamic properties of water result from hydrogen bonding.[3] Linear and nonlinear vibrational spectroscopies are a very common tool to study the properties of hydrogen bonds,[4,5] and often reveal results that are very peculiar and very different from any other vibrational mode. That is, vibrational bands of OH or NH-groups involved in hydrogen bonds are typically very broad and exhibit strong red shifts as compared to the non-hydrogen bonded case. The prototype example is the OH-stretch vibration of liquid water, where both broadening and solvation shift are a few 100 cm^{-1}, as opposed to typically 10 cm^{-1} of "normal" vibrational modes. Furthermore, if a hydrogen bond is of intramolecular nature,[6–8] binding a dimer with reasonably well defined structure,[9,10] or in hydrogen-bonded molecular crystals,[11,12] the vibrational band often contains a pronounced substructure. The nonlinear pump-probe response of these infrared (IR) transitions, in turn, often decays on an ultrafast (a few 100 fs) time scale[13–15] and in some cases also exhibits complex oscillatory features.[6–12] It is the very anharmonic nature of the hydrogen bond potentials that gives rise to the peculiar vibrational spectroscopy,[16–22] i.e., in essence the fact that the typical dissociation energy of a hydrogen bond is in the same range as the frequency of its vibrational modes. It has also been shown that the problem is inherently high-dimensional,[17–22] which renders the modeling of the quantum dynamics demanding and the interpretation of the computational results complicated.

In a series of papers, Johnson and coworkers have investigated hydrogen bonded complexes of a water molecule with various molecular ions such as NO_2^-, HCO_2^-, $CH_3NO_2^-$, and $CH_3CO_2^-$ in the gas phase by Ar-tag IR spectroscopy.[18,23–26] In addition in related work, Neumark and coworkers have studied the complex with NO_3^-.[27] Despite the fact that these complexes show all the nontrivial features of the IR spectroscopy of hydrogen bonds, their spectral signatures are particularly simple. That is, the OH stretch vibration of the water molecule splits into a single pronounced "Franck-Condon"-like progression due to the strong anharmonic coupling to the water rocking mode.[18,22,23] Furthermore, this Franck-Condon progression sits on a broad background that might indicate an ultrafast relaxation channel. While the Franck-Condon progression has been reproduced using cubic *ab initio* derived force constants,[18,22] the broad background and its underlying dynamics still awaits an explanation. Owing to the smallness of these complexes, one can treat both their quantum chemistry as well as their quantum dynamics on a reasonably high level that should lead to a qualitatively correct picture of the underlying mechanism.

We have recently introduced the concept of vibrational conical intersections[28,29] as a possible mechanism for ultrafast

vibrational relaxation, just like it is for the electronic case.[30–32] The very concept of a conical intersection requires an adiabatic separation of time scales of two sets of degrees of freedom, which is naturally given in the electronic case via the Born-Oppenheimer approximation, but which is less common for vibrational transitions.[18,20,22,33–36] In the context of vibrational conical intersections, an adiabatic separation has been introduced between high-frequency OH stretch and bend vibrations on the one hand, and lower-frequency backbone vibrations[28] or torsional modes[37,38] on the other hand within one molecule. Alternatively, in the case of the hydrogen-bonded water dimer, the high-frequency intramolecular modes have been separated from the lower-frequency intermolecular modes.[29] Hydrogen-bonded complexes are particularly likely to reveal vibrational conical intersections, since the change of its intermolecular configuration leads to comparably large tunings of the OH-stretch vibrations involved in the hydrogen bond, that is, the very effect that gives rise to the peculiar spectroscopic properties discussed above.

Applying this adiabatic approach, in this work we study theoretically the vibrational relaxation dynamics and resulting spectral signature of one of the complexes introduced by Johnson and coworkers, $HCO_2^-\cdot H_2O$.[26] We chose that particular complex because of its smallness and its high C_{2v} symmetry. $NO_2^-\cdot H_2O$, which would be even smaller, has been discarded since its C_{2v} structure is not the lowest energy structure.[23] $HCO_2^-\cdot H_2O$ exhibits the same Franck-Condon-like progression as the other clusters in addition to a broad background (see supplementary material of Ref. 26 and Fig. 8(c)), the latter of which, however, being less pronounced as compared to complexes with either $CH_3NO_2^-$ or $CH_3CO_2^-$.[23] Including three intramolecular and three intermolecular degrees of freedom, we explore the coherent (i.e., oscillatory) population transfer after excitation of the OH-stretch vibration into the HOH-bend overtone, which is in close resonance and coupled to the OH-stretch vibration by a conical intersection. Furthermore, relaxation into the HOH-bend fundamental and the ground state is observed, which occurs in an incoherent (i.e., exponential) manner. Although this second relaxation is not facilitated by any curve crossing, its time scale is not significantly slower than that of the first coherent process. We close with a discussion of the virtues and limitations of the adiabatic ansatz to interpret vibrational dynamics.

II. THEORY AND METHODS

A. Separation of fast and slow vibrations

In direct analogy, the Born-Oppenheimer approach to separate electronic and nuclear degrees of freedom, we partition the vibrations into high-frequency modes $q = \{q_i\}$ and low-frequency modes $Q = \{Q_j\}$. This yields the Hamiltonian

$$H = T_q + T_Q + V(q,Q), \tag{1}$$

where T_q and T_Q denote the kinetic energy of the high- and low-frequency modes, respectively, and $V(q,Q)$ represents the potential energy surface (PES) of these vibrations in the electronic ground state. The time-dependent Schrödinger equation for the system reads

$$i\hbar\frac{\partial}{\partial t}|\Psi(t)\rangle = H|\Psi(t)\rangle. \tag{2}$$

Fixing the low-frequency modes $\{Q_j\}$ to a constant value, we first solve the Schrödinger equation for the high-frequency modes,

$$\left[T_q + V(q,Q) - W_n^{\mathrm{ad}}(Q)\right]|\psi_n^{\mathrm{ad}}\rangle = 0, \tag{3}$$

which yields the *vibrational* adiabatic states $|\psi_n^{\mathrm{ad}}\rangle$ and the corresponding adiabatic PESs $W_n^{\mathrm{ad}}(Q)$. As the states $|\psi_n^{\mathrm{ad}}\rangle$ represent a complete basis set for the high-frequency modes, we can expand the total vibrational wave function,

$$|\Phi(Q)\rangle = \sum_n \chi_n^{\mathrm{ad}}(Q)|\psi_n^{\mathrm{ad}}\rangle, \tag{4}$$

where the wave functions $\chi_n^{\mathrm{ad}}(Q)$ account for the dynamics of the low-frequency modes on the various PESs. Insertion into the Schrödinger equation for the total Hamiltonian [Eq. (1)] yields the coupled-channel equations,

$$\left[T_Q + W_n^{\mathrm{ad}}(Q) - E\right]\chi_n^{\mathrm{ad}}(Q) = \sum_m \Lambda_{nm}\chi_m^{\mathrm{ad}}(Q), \tag{5}$$

where the operator Λ_{nm} accounts for the nonadiabatic coupling between the adiabatic vibrational states $|\psi_n^{\mathrm{ad}}\rangle$ and $|\psi_m^{\mathrm{ad}}\rangle$. In the commonly used adiabatic approximation, one assumes that $\Lambda_{nm} = 0$, which leads to independent low-frequency vibrational dynamics on the adiabatic PESs $W_n^{\mathrm{ad}}(Q)$.

Due to the presence of kinetic couplings containing derivatives, the computation of the nonadiabatic coupling matrix $\{\Lambda_{nm}\}$ is quite tedious. Usually, one therefore changes to a *diabatic* representation with states $|\psi_m^{\mathrm{dia}}\rangle$, which are related to the adiabatic states via a unitary transformation. In the diabatic representation, the kinetic couplings vanish at the expense of a nondiagonal potential energy matrix $\mathcal{V}^{\mathrm{dia}}$, resulting in the diabatic Hamiltonian

$$\mathcal{H}^{\mathrm{dia}} = T_Q\mathbf{1} + \sum_{n,m}|\psi_n^{\mathrm{dia}}\rangle\mathcal{V}_{nm}^{\mathrm{dia}}\langle\psi_m^{\mathrm{dia}}|. \tag{6}$$

Employing a time-dependent formulation, the Schrödinger equation of the coupled system in the diabatic representation reads

$$i\hbar\frac{\partial}{\partial t}|\Psi(t)\rangle = \mathcal{H}^{\mathrm{dia}}|\Psi(t)\rangle, \tag{7}$$

where

$$|\Psi(t)\rangle = \sum_m \chi_m^{\mathrm{dia}}(Q,t)|\psi_m^{\mathrm{dia}}\rangle \tag{8}$$

represents the time-dependent state vector in the diabatic representation. The wave function $\chi_m^{\mathrm{dia}}(Q,t)$ is the main quantity of interest as it describes the vibrational dynamics of the low-frequency modes $\{Q_j\}$ on the coupled PESs $\mathcal{V}_{nm}^{\mathrm{dia}}$ generated by the high-frequency modes $\{q_i\}$. From the time-dependent propagation of $|\Psi(t)\rangle$, we calculate the time-dependent population probabilities of the diabatic states,

$$P_m(t) = |\langle\Psi(t)|\psi_m^{\mathrm{dia}}\rangle|^2 = \langle\chi_m^{\mathrm{dia}}(t)|\chi_m^{\mathrm{dia}}(t)\rangle, \tag{9}$$

which are a key quantity to discuss the vibrational relaxation dynamics of the system, as $P_m(t) = const.$ in the absence of coupling.

B. Definition of inter- and intramolecular coordinates

As a first step, we need to choose suitable coordinates for the intramolecular high-frequency modes $\{q_i\}$ and intermolecular low-frequency modes $\{Q_j\}$ of $HCO_2^-\cdot H_2O$. Rather than using the normal modes of the complex directly, which has been shown to reveal a very poor adiabatic representation,[29] we use "internal coordinates," where the intramolecular coordinates are the normal modes of either the H_2O or the HCO_2^- monomer, which move (rotate) as the molecules moves (rotates) in the complex along the intermolecular modes. The intermolecular coordinates $\{Q_j\}$, on the other hand, are curvilinear coordinates that keep the individual molecules rigid. As described in detail in Ref. 29, their linearisations for small displacements are mapped onto the corresponding Cartesian normal mode coordinates.

From the nine intra-molecular modes, we considered only those of the water molecule, for which strongly anharmonic effects in their line shapes have been observed experimentally.[23] That is, we considered the two OH-stretch modes of the water molecule (q_1 and q_2, which we define as local modes rather than the symmetric and asymmetric stretch vibrations, see Fig. 1(a)), as well as the HOH bending mode (q_3) because of its Fermi-resonance with the OH stretching modes. Of the total six intermolecular modes, on the other hand, we considered only the three in-plane modes Q_1, Q_2, and Q_3 depicted in Fig. 1(b), as they tune the frequencies of the water molecule's intramolecular modes as a function of mode displacement by far more than the out-of-plane modes. All coordinates $\{Q_j\}$ and $\{q_i\}$ are defined in dimensionless normal mode units (to that end, the curvilinear coordinates $\{Q_j\}$ have been scaled such that they agree for small displacements with the corresponding normal modes defined in dimensionless units).

C. Quantum-chemical calculations

Based on the above defined coordinates, we next wish to calculate the potential energy $V(q,Q)$ of Hamiltonian (1). To this end, we performed *ab initio* calculations at the MP2/aug-cc-pvdz level of theory (which is the same level of theory as in Ref. 18), using the Gaussian09 program package.[39] Intending to exploit a separation between high-frequency modes $\{q_i\}$ and low-frequency modes $\{Q_j\}$, we first calculate the potential energy $V(q;Q)$ as a function of the $\{q_i\}$, assuming a given set of intermolecular coordinates $\{Q_j\}$, i.e., for a given configuration of the two molecules with respect to each other. For each such configuration, the positions $\{q_i\}$ of all intramolecular modes, including those of the HCO_2^- molecule, have first been minimized. Using that minimum-energy point $\{q_i^{(0)}\}$ as origin, the potential energy is power-expanded as a function of the three H_2O modes q_1, q_2, and q_3 via

$$V(q;Q) = \sum_{i,j,k=0}^{4} a_{ijk}\, \delta q_1^i\, \delta q_2^j\, \delta q_3^k + \sum_{l=1}^{3} b_l\, \delta q_l^5, \quad (10)$$

where $\delta q_n = q_n - q_n^{(0)}$ and the coefficients a_{ijk} and b_l, as well as the minima $\{q_i^{(0)}\}$ are functions of Q. Coefficients a_{ijk} with $i+j+k=1$ are zero since the potential energy is expanded around its minimum $(q_1^{(0)}, q_2^{(0)}, q_3^{(0)})$. The resulting 125 nonzero coefficients a_{ijk} and b_l were determined by inversion from 125 single point quantum-chemical calculations. To determine the positions of these 125 points, we started from a $5\times5\times5$ cube centered around the origin and then modified the distance of each point to the origin such that two ellipsoids were obtained. The inner ellipsoid contained $3^3-1=26$ points, the outer ellipsoid $5^3-27=98$ points. The radius of the inner ellipsoid was 1.6 in the q_1 and q_2 directions and $1.6\cdot\sqrt{2}$ in the q_3 direction (since the first overtone is most relevant for the HOH bend mode) and that of the outer ellipsoid 3.0 and $3.0\cdot\sqrt{2}$, respectively. These radii were chosen to minimize the error in the energy of the OH stretch fundamentals and the HOH bend overtone.

Using a harmonic-oscillator basis $\{|n_i\rangle\}$ to represent the high-frequency modes $\{q_i\}$ and standard creation $(\hat{a}_i^\dagger)$ and annihilation $(\hat{a}_i)$ operators, the matrix elements of the corresponding Hamiltonian of the high-frequency modes are readily constructed. A "pruned" basis[40] including up to 8 quanta for the OH stretch vibrations and 16 quanta for the HOH vibration was used for this purpose, resulting in 285 basis states. Due to the quintic terms, potential Eq. (10) is unbounded from below in principle. We have verified that the limited basis with maximal 8 quanta in the OH stretch or 16 quanta for the HOH bend does, however, not yet explore regions of the potential energy surface where the potential turns over and diverges towards $-\infty$. The size of the basis together with the power expansion of the PES [Eq. (10)] results in a convergence of the eigenfrequencies of the OH stretch states $|1,0,0\rangle$ and $|0,1,0\rangle$ and the HOH bend first overtone $|0,0,2\rangle$ of $\lesssim$10 cm^{-1}, which for a selection of Q-points has been verified against a much denser q-grid and a much larger basis $\{|n_i\rangle\}$.

The above described calculation of the potential energy $V(q;Q)$ needs to be done for all low-frequency positions $Q = (Q_1, Q_2, Q_3)$ of interest. Since the PES is highly anharmonic in Q-space, a power expansion as done for the q-space [Eq. (10)] is not feasible. Alternatively, we use a discrete value representation (DVR),[41] which requires that the PESs are calculated on an equidistant grid. The DVR also facilitates a computationally inexpensive calculation of the kinetic energy operator T_Q.[42] Since the final goal is to calculate the vibrational relaxation from the initially excited OH-states cascading down

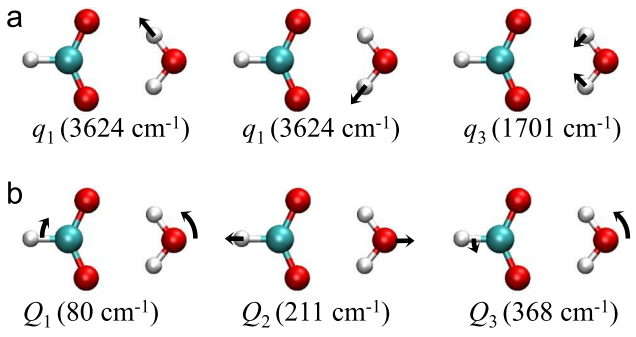

FIG. 1. Vibrational modes of $HCO_2^-\cdot H_2O$ considered in this study: (a) intramolecular high-frequency modes and (b) intermolecular low-frequency modes. The harmonic frequencies are given in parenthesis; in the case of the two stretch vibrations, the average of the symmetric (3619 cm^{-1}) and asymmetric (3629 cm^{-1}) stretch frequencies is given.

via the HOH-bend into the ground state, we need to converge Q-basis on the ground state surface up to the regime of the excitation energy. On the one hand, this determines the grid spacing needed to converge the kinetic energy, for which we chose $\Delta Q_1 = 0.3$, $\Delta Q_2 = 0.4$, and $\Delta Q_3 = 0.5$. On the other hand, it requires that grid points up to at least that energy regime are included. As the overall calculation becomes computationally expensive, we cannot use a cuboid-shaped three-dimensional grid, but rather extend the grid step-wise in all three dimensions, starting from the origin, until the energy of the ground state exceeded 3500 cm^{-1} (plus zero-point energy). This procedure results in 108 824 grid points, only half of which have to be calculated explicitly owing to the symmetry of the molecular complex.

D. Representation of the wave function

As outcome of the above introduced formulation, we may express the total vibrational wave function as

$$|\Phi(Q)\rangle = \sum_{k,n_1,n_2,n_3} c^{(k)}_{n_1 n_2 n_3}\, \xi_k(Q_1,Q_2,Q_3)\, |n_1\rangle|n_2\rangle|n_3\rangle, \tag{11}$$

where the harmonic-oscillator states $\{|n_i\rangle\}$ represent the high-frequency modes $\{q_i\}$ and the DVR basis functions $\{\xi_k\}$ represent the low-frequency modes $\{Q_j\}$. Within our model assumptions (i.e., restriction to six modes and convergence of basis sets), Eq. (11) constitutes the numerically exact representation of the vibrational wave function. With a total number of $285 \times 108\,824 \approx 3 \times 10^7$ basis functions, however, the propagation of corresponding time-dependent Schrödinger equation (2) is quite tedious.

To significantly reduce the basis size of the problem, we may exploit the time scale separation of fast and slow vibrations explained in Sec. II A and represent the high-frequency modes $\{q_i\}$ in terms of a few diabatic eigenstates $|\psi_n^{\rm dia}\rangle$ (instead of 285 harmonic-oscillator states). For the discussion below, we restricted the state space to five states, that is, the overall ground state $|0,0,0\rangle$, the fundamentals $|1,0,0\rangle$ and $|0,1,0\rangle$ of the two OH stretch vibrations, and the fundamental $|0,0,1\rangle$ and the first overtone $|0,0,2\rangle$ of the HOH bend vibration. Using the harmonic-oscillator basis $\{|n_i\rangle\}$, we first calculated the adiabatic eigenstates $|\psi_n^{\rm ad}\rangle$ and the corresponding adiabatic PESs $W_n^{\rm ad}(Q)$ by solving the Schrödinger equation for the high-frequency modes, Eq. (3).

As a simple means to introduce diabatic basis states, we employ a vibrational self-consistent field (VSCF) approach.[43] VSCF wave-functions can be viewed as an approximate diabatic representation, in the sense that they do not change their character even when the energies of two states cross as a function of Q, i.e., $\partial\psi_m^{\rm dia}/\partial Q_j$ remains small. For a given intermolecular configuration (Q_1,Q_3,Q_3), the VSCF wave-functions are expressed as a product ansatz,

$$\psi_m^{\rm dia}(q) = \phi_{j1}(q_1)\, \phi_{j2}(q_2)\, \phi_{j3}(q_3), \tag{12}$$

where $\phi_{ji}(q_i)$ describes the jith eigenstate of high-frequency mode q_i, with $m = (j1, j2, j3)$ representing the corresponding quantum numbers. To construct the diabatic states $|\psi_m^{\rm dia}\rangle$, we iteratively and self-consistently solved the one-dimensional Schrödinger equations[44]

$$\left[\frac{\omega_i}{2}\hat{p}_i^2 + \overline{V}_i(q_i)\right]\phi_{ji} = E_{ji}\phi_{ji} \tag{13}$$

with

$$\overline{V}_i(q_i) = \left\langle \prod_{k\neq i}\phi_{jk}\middle| V(q;Q)\middle|\prod_{k'\neq i}\phi_{jk'}\right\rangle. \tag{14}$$

As an initial guess of $\overline{V}_i(q_i)$ for the first step of the VCSF iteration, we used the corresponding harmonic states.

To construct the diabatic Hamiltonian in Eq. (6), we want to expand the adiabatic eigenstates $|\psi_n^{\rm ad}\rangle$ defined in Eq. (3) in the basis of diabatic states $|\psi_m^{\rm dia}\rangle$ defined above. When doing so, one needs to keep in mind that the set of the diabatic states does not exactly represent an orthonormal basis. Furthermore, the space spanned by these basis states does not completely cover that of the adiabatic states. As a consequence, the matrix

$$C_{mn} = \langle\psi_m^{\rm dia}|\psi_n^{\rm ad}\rangle \tag{15}$$

is not unitary, albeit very close to it with the elements of the overlap matrix $\mathcal{S} = C^T C$ being $\mathcal{S}_{nn} \gtrsim 0.995$ and $\mathcal{S}_{nm} \lesssim 0.0005$ for $n \neq m$. In order to orthogonalize the basis, we calculate $\mathcal{S}^{-1/2}$ and introduce the unitary matrix $\mathcal{U} \equiv \mathcal{S}^{-1/2}C$. With that, the diabatic potential energy matrix $\mathcal{V}^{\rm dia}$ is given by

$$\mathcal{V}^{\rm dia} = \mathcal{U}\, \mathcal{W}^{\rm ad}\, \mathcal{U}^T, \tag{16}$$

where $\mathcal{W}^{\rm ad}$ is a diagonal matrix containing the adiabatic energies $W_n^{\rm ad}$ from Eq. (3). The diagonal elements of the matrix $\mathcal{V}^{\rm dia}$ contain the energies of the corresponding diabatic states (which differ by some 10 cm^{-1} from those obtained from Eq. (13), since the set of diabatic states is not a complete basis), and the off-diagonal elements reflect the nonadiabatic couplings between them. Diagonalization of $\mathcal{V}^{\rm dia}$ reproduces the adiabatic states by construction.

E. Vibrational dynamics

Finally, we are in a position to propagate the time-dependent Schrödinger equation of the coupled vibrational dynamics of the high- and the low-frequency modes. This is done for two different models using two different levels of theory. First, we consider a 3-state model including the fundamentals $|1,0,0\rangle$ and $|0,1,0\rangle$ of the two OH stretch vibrations and the closely resonant first overtone $|0,0,2\rangle$ of the HOH bend vibration. Adopting the above introduced diabatic representation of these states, we will discuss curve crossings, vibrational energy redistribution, and the associated vibrational spectra of this system.

To also study the subsequent vibrational relaxation into the HOH bend fundamental $|0,0,1\rangle$ and the ground state $|0,0,0\rangle$, we consider a 5-state model that additionally includes these two states, which are separated by $\approx$1700 cm^{-1} and $\approx$3400 cm^{-1} from the higher-lying states, respectively. While the diabatic representation is still appropriate for calculating the PESs of these states, it turns out that a diabatic picture describes only poorly the nonadiabatic couplings relevant for vibrational relaxation into the lower states, as other nonadiabatic coupling mechanisms take over due to the

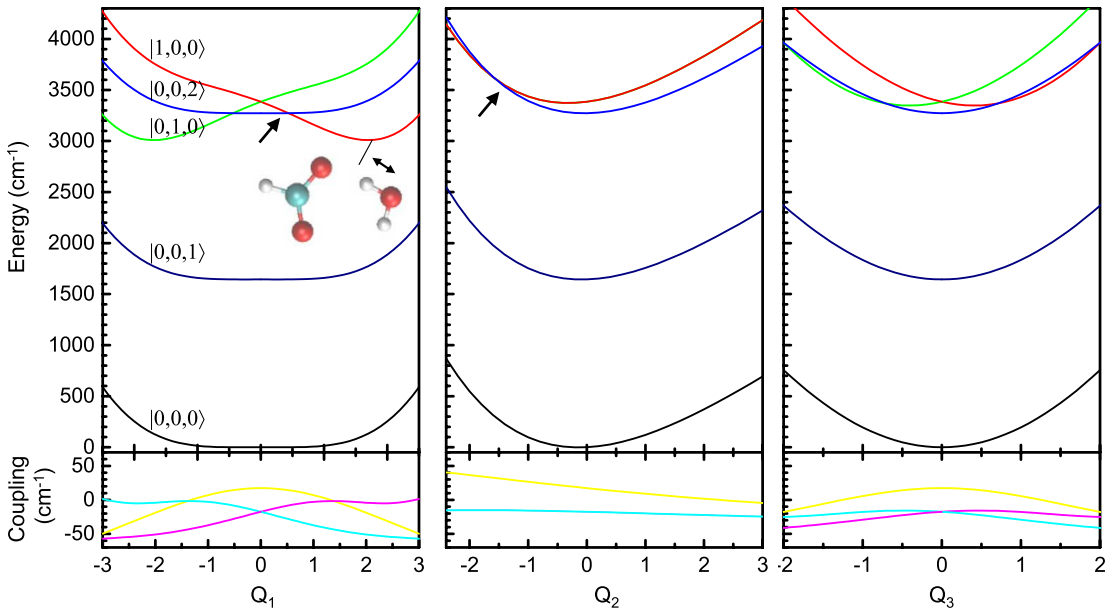

FIG. 2. One-dimensional cuts of the diabatic potential energy surfaces as a function of the three intermolecular degrees of freedom Q_1, Q_3, Q_3 with the corresponding other coordinates fixed at zero. Upper panels: the ground state surface $|0,0,0\rangle$ is shown in black, the HOH bend fundamental $|0,0,1\rangle$ in navy, the two OH stretches in red ($|1,0,0\rangle$) and green ($|0,1,0\rangle$), respectively, and the HOH bend overtone $|0,0,2\rangle$ in blue. Along Q_2, the two OH stretch surfaces are degenerate and only the red one is shown. Zero-point energy (4390.7 cm^{-1}) has been subtracted, i.e., the ground state energy surface at the origin is set to 0. The structure of the complex at the minimum of the $|1,0,0\rangle$ surfaces is shown. The arrows in the left and middle panel indicate conical intersections discussed in the text. Lower panels: diabatic couplings between the active states are color-coded consistently in the sense of a RGB color code, that is, the coupling between the two OH stretch surfaces (red *versus* green) is colored in yellow, the coupling between the red OH stretch surface and the blue HOH bend overtone in magenta, and that between the green OH stretch surface and the blue HOH bend overtone in cyan.

large energy spacing. In particular, the diabatic representation does not account for the Q-dependence of the minima $\{q_i^{(0)}\}$ in the potential-energy expansion [Eq. (10)], which dominates the nonadiabatic couplings between the initially excited states and the HOH-bend fundamental as well as the ground state.[45] To avoid these problems, we perform a numerically exact propagation of the total vibrational wave function [Eq. (11)]. While being much more expensive (about a factor of 150) than the corresponding diabatic calculation, we thus obtain a numerically exact solution of the Schrödinger equation, which implicitly includes all nonadiabatic couplings.

For both models, we need to define the initial wave-function of the system at time $t = 0$. To this end, we first calculated the wave-function of the vibrational ground state $|0,0,0\rangle$ by using an iterative Lanczos algorithm. In order to mimic a vertical Franck-Condon transition into the symmetric OH-stretch vibration, the ground state wave-function was then projected onto $1/\sqrt{2}(|1,0,0\rangle + |0,1,0\rangle)$. Using that wave-function as initial condition, time-dependent Schrödinger equation (2) or (7) was propagated, using a Chebychev scheme to calculate the required matrix-exponentials.[46]

III. RESULTS

A. Potential energy surfaces

1. Franck Condon region

Let us first discuss the PESs of the 5-state model, that account for the ground state $|0,0,0\rangle$, the two OH stretch fundamentals $|1,0,0\rangle$ and $|0,1,0\rangle$, and the first and second HOH bend excitation $|0,0,1\rangle$ and $|0,0,2\rangle$. One-dimensional cuts of the diabatic PESs are shown in Fig. 2 with the corresponding other coordinates fixed at zero. The origins of coordinates Q_1, Q_2, and Q_3 correspond to the minima of the Born-Oppenheimer surface (which is not shown in Fig. 2). In the case of Q_1 and Q_3, these minima coincide with that of the $|0,0,0\rangle$ ground state surface owing to symmetry, while the minimum of Q_2 is slightly shifted to $Q_2 = -0.2$ due to zero-point energy effects. In any case, the minima of the three coordinates represent the Franck Condon point.

Mode Q_1 is the strongest tuning coordinate;[47] that is, the bottom of the $|1,0,0\rangle$ surface at 3009 cm^{-1} is displaced by $Q_1 = 1.7$ and lies 375 cm^{-1} below the vertical "Franck-Condon" energy of 3384 cm^{-1} at $Q_1 = 0$. The minimum is related to a structure which breaks the symmetry of the complex, and in which the excited OH stretch vibration forms a tighter hydrogen bond (see Fig. 2, left panel). When searching the minimum of the $|1,0,0\rangle$ surface in all three dimensions, it is even a bit lower with 2950 cm^{-1} at $(Q_1, Q_2, Q_3) = (2.7, 1.2, -0.5)$.

The ground state surface is essentially flat along Q_1 for a pretty large range, which results from the fact that the positive curvature of the Born-Oppenheimer surface (not shown; its harmonic frequency is 80 cm^{-1}) is counterbalanced by the decreasing zero-point contribution of states $|1,0,0\rangle$ and $|0,1,0\rangle$ to the ground state surface. The HOH-bend fundamental $|0,0,1\rangle$ and first overtone $|0,0,2\rangle$ surfaces are mostly parallel to the ground state surface, hence the HOH-bend frequency is essentially independent of the molecular configuration of

the cluster. No curve crossings exist between the HOH-bend fundamental $|0,0,1\rangle$ and the OH-stretch states $|1,0,0\rangle$ or $|0,1,0\rangle$.

2. Conical intersection seam

Owing to the large tunings of the OH-stretch modes as a function of $\{Q_j\}$, a rich set of curve crossings appear for the states $|1,0,0\rangle$, $|0,1,0\rangle$, and $|0,0,2\rangle$. For example, on the way from the Franck-Condon point to the minimum, the $|1,0,0\rangle$ state crosses the HOH-bend overtone $|0,0,2\rangle$ (see arrow in Fig. 2, top-left panel). The states are coupled with coupling constants that lie in a range of $\approx\pm 50$ cm^{-1} (Fig. 2, lower panels), hence that crossing is in fact a weakly avoided crossing. But there are true conical intersections between these three states. In particular, the arrow in the middle panel of Fig. 2 marks a symmetry-allowed conical intersection between the HOH-bend overtone (which is an A_1 mode) and the asymmetric OH stretch vibration (B_2). It extends into a one-dimensional conical intersection seam in (Q_1,Q_3,Q_3)-space between the two lowest adiabatic states, i.e., between the HOH-bend overtone and the lower one of the OH-stretch modes, when breaking the symmetry of the complex along the Q_1 and/or Q_3 directions. The conical intersection seam has been calculated using a steepest decent algorithm,[48] minimizing the adiabatic energy difference between both states. As initial values, random points in (Q_1,Q_3,Q_3)-space were chosen and convergence was assumed once the energy difference dropped below 0.001 cm^{-1}. To that end, the diabatic potential energy and coupling surfaces V^{dia}, which are smooth functions in Q, were calculated on an equidistant grid with $\Delta Q = 0.2$ and approximated in between by a 3rd-order interpolation. The results are shown in Fig. 3. Parts of the conical intersection seam are in fact below the Franck Condon energy (see dotted line in Fig. 3(a) and blackish colors in both panels), and they are likely to be reached by a wave packet launched from the Franck-Condon point.

3. Hydrogen bonded isomers

When exploring the PESs further out, they become remarkably complex (see Fig. 4), since there are other hydrogen bonded isomers in addition to the C_{2v} structure. That is, there are two "backside" hydrogen-bonded forms[24,25] at $(Q_1,Q_2,Q_3) = (15.6, 6.5, -17.5)$ and $(Q_1,Q_2,Q_3) = (16.6, 6.8, -10)$ with energies of 610 cm^{-1} and 660 cm^{-1}, respectively, relative to the minimum of the ground state surface. In both cases, the energy drops below the Frank-Condon energy when exciting the corresponding OH-stretch vibration, so they are, in principle, energetically accessible after IR excitation. But the height of the barriers separating these minima from the Franck-Condon region is $\gtrsim$1200 cm^{-1}, hence tunneling through them will be small. A third minimum is found at $(Q_1,Q_2,Q_3) = (3.6, 4.8, -8.5)$, in which one of the OH-groups of the water is hydrogen bonded to the opposite oxygen atom of HCO_2^-. With 1020 cm^{-1} for the ground state surface, that minimum is somewhat higher in energy.

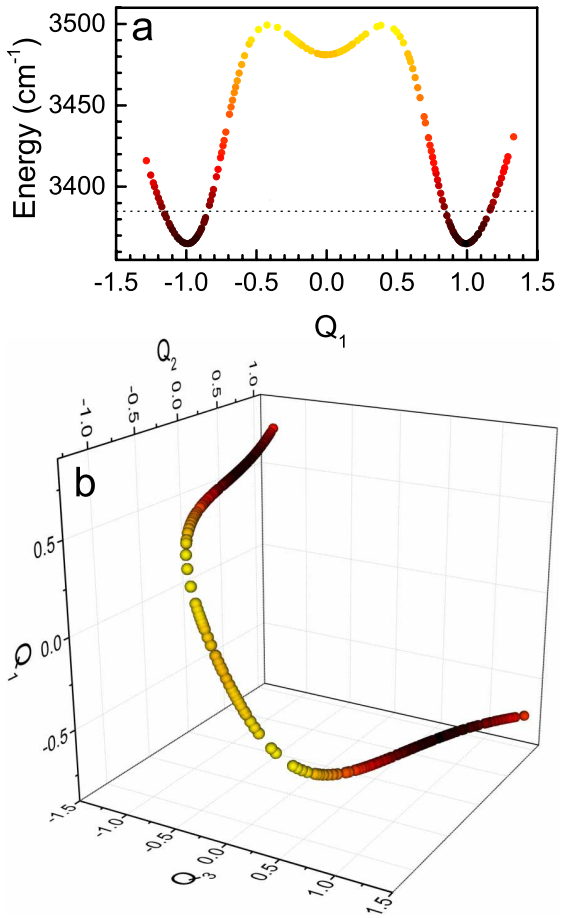

FIG. 3. (a) Energy of the conical intersection seam between the PESs of the HOH-bend overtone and the asymmetric OH stretch vibration as a function of Q_1. The dotted line indicates the Franck-Condon energy (with the zero-point energy 4390.7 cm^{-1} subtracted), and the colors the energy of the conical intersection with blackish colors being below the Franck-Condon energy. (b) Position of the conical intersection seam in (Q_1,Q_2,Q_2) space. The color code is the same as in panel (a).

B. Vibrational dynamics

1. Vibrational dynamics of the 3-state model

We first consider the above introduced 3-state model comprising the excited states $|1,0,0\rangle$, $|0,1,0\rangle$, and $|0,0,2\rangle$. A diabatic representation of these states is used to describe the system's vibrational dynamics according to time-dependent Schrödinger equation (7). From the propagation of this equation, we calculate the time-dependent population probabilities of the diabatic states $P_m(t)$ defined in Eq. (9), which are shown in Fig. 5(a). The population of the HOH-bend overtone $|0,0,2\rangle$ jumps to $\approx$3%-4% within the first 60 fs in a first transfer step, and to $\approx$12% after 500 fs in a second step (see Fig. 5(a), inset). That is, each time the wave-packet, illustrated by the expectation value of Q_2 (see Fig. 5(b)), passes by the conical intersection seam, a small fraction of the wave-packet is transferred from the initially excited OH stretch state $1/\sqrt{2}(|1,0,0\rangle + |0,1,0\rangle)$ into the optically dark HOH-bend overtone $|0,0,2\rangle$, just like for curve crossings between electronic states.[49] On a longer time scale, the dynamics remains oscillatory with a major period of $\approx$2-2.5 ps, but the population of the

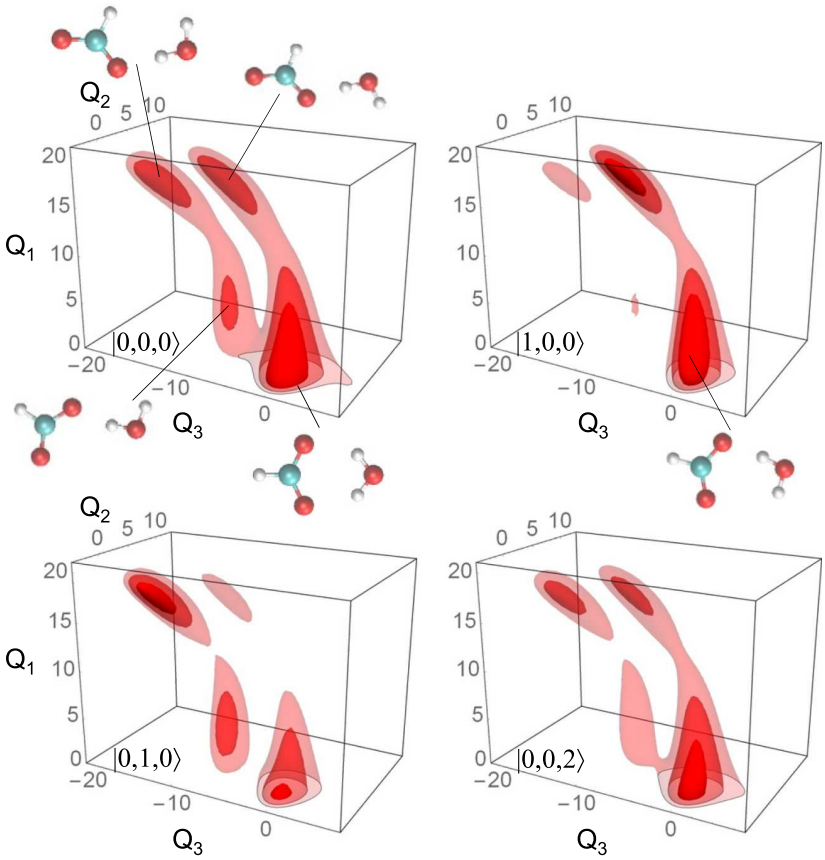

FIG. 4. Three-dimensional representation of the diabatic potential energy surfaces for the ground state $|0,0,0\rangle$, the OH-stretches $|1,0,0\rangle$ and $|0,1,0\rangle$, as well as the HOH-bend overtone $|0,0,2\rangle$ (the HOH-bend fundamental is not shown as it is very similar to the HOH-bend overtone, apart from an energy shift). Three contour surfaces separated by 600 cm^{-1} are shown with increasing degree of transparency. The origin of these contour surfaces is the minimum of the $|0,0,0\rangle$ surface for the top-left panel, and the minimum of the $|1,0,0\rangle$ surface for all other panels. The structures of the complex in the various local minima are indicated. The negative Q_1-space is related to the positive one by the symmetry of the molecule.

HOH-bend overtone never drops below the value after the first transfer step (3%-4%), hence, that step is irreversible. The coherent population transfer to the HOH-bend overtone $|0,0,2\rangle$ can be considered the time-domain analog of a Fermi-resonance, which is commonly believed to play an important role in the vibrational dynamics of hydrogen-bonded systems.[50–53] While the coherent wave packet motion on diabatic PESs can be measured in time-resolved pump-probe experiments,[54,55] the population dynamics in the adiabatic representation does not necessarily exhibit strongly oscillatory behavior.

2. Vibrational dynamics of the 5-state model

We now consider the complete 5-state model, which additionally includes the HOH bend fundamental $|0,0,1\rangle$ and the ground state $|0,0,0\rangle$ of the system. As explained in Sec. II E, for this case we need to employ a numerically exact propagation scheme, which implicitly includes all nonadiabatic couplings. As shown in Fig. 5(c), the results are very similar with respect to the step-wise increase of the population of the HOH-bend overtone $|0,0,2\rangle$ during the first picosecond, which indicates that the diabatic calculation of Fig. 5(a) indeed describes the nonadiabatic couplings within the 3-state model reasonably well. On a somewhat longer time scale, the population now cascades from the OH-stretch states $1/\sqrt{2}(|1,0,0\rangle + |0,1,0\rangle)$ via the HOH-bend overtone $|0,0,2\rangle$ and the fundamental $|0,0,1\rangle$ into the ground state $|0,0,0\rangle$. That is, the HOH-bend fundamental $|0,0,1\rangle$ (see Fig. 5(c), inset, green line) picks up population only after the first 60 fs jump of population into the HOH-bend overtone $|0,0,2\rangle$ (blue line) has occurred. It is, however, only a very small amount of population in the HOH-bend overtone $|0,0,2\rangle$ that is needed to funnel it into the HOH-bend overtone $|0,0,1\rangle$, as the populations of both states rise in parallel on a somewhat longer time scale. The population rise of the ground state $|0,0,2\rangle$ (black line), in turn, has a larger lag time and requires population to first accumulate in the HOH-bend overtone $|0,0,1\rangle$.

In contrast to the dynamics between the OH stretch mode and the HOH-bend overtone, relaxation proceeds in essentially an exponential—rather than a coherent—manner. Note that no empirical relaxation term or bath has been included in the simulation; the system is modeled as a closed quantum system. A bi-exponential fit of the decay of the OH-stretch relaxation (considering data up to 32.8 ps, not all of which are shown in Fig. 5(c)) reveals time constants of 0.5 ps (amplitude 0.15) and 3.8 ps (amplitude 0.22), as well as a constant offset at 0.13. The time scales are quite typical for the relaxation of a vibrational mode.[13–15]

Fig. 6 shows the time evolution of kinetic energy of the low-frequency vibrations in the $|0,0,0\rangle$ ground state. Initially, the rate of pickup of kinetic energy differs between the three low-frequency modes, with Q_3 being the fastest, probably since it is the mode with highest frequency and as such requires the smallest change in quantum numbers. On the other hand, the lowest frequency mode Q_1 is not the slowest, since its coupling to the OH-stretch state $|1,0,0\rangle$ is the strongest (Fig. 2). Interestingly, the kinetic energy of all three modes

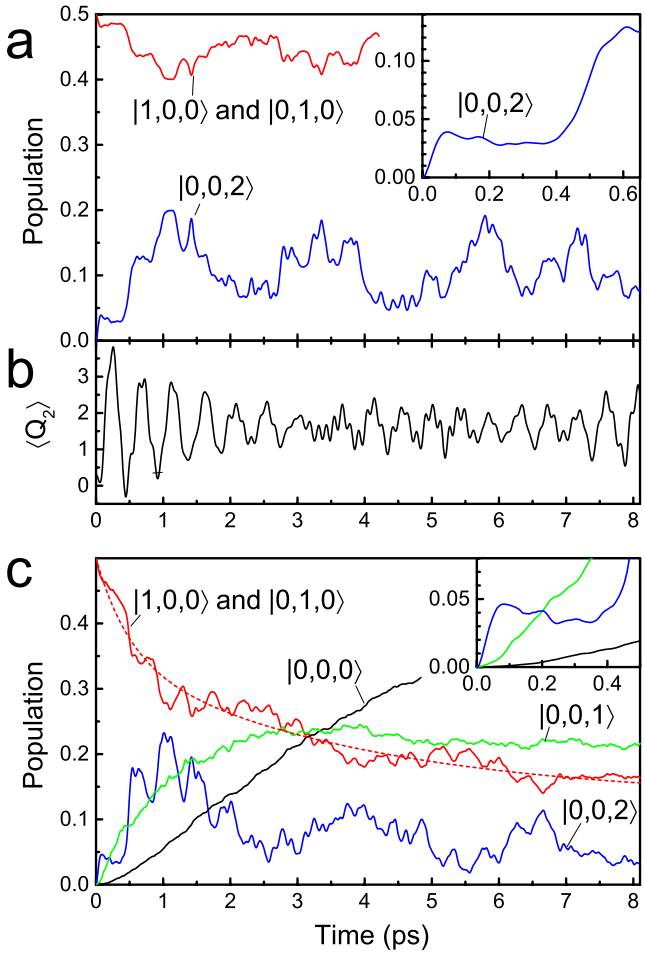

FIG. 5. (a) Vibrational relaxation dynamics of the 3-state model calculated in a diabatic representation. Shown are the time-dependent population probability of the OH-stretch fundamental ($|1,0,0\rangle$, red) and the HOH-bend overtone ($|0,0,2\rangle$, blue), following impulsive excitation of the symmetric OH-stretch vibration, $1/\sqrt{2}(|1,0,0\rangle + |0,1,0\rangle)$. The populations of states $|1,0,0\rangle$ and $|0,1,0\rangle$ stay the same at all times, hence only the former is shown. (b) Time-dependent expectation value of Q_2. (c) Vibrational relaxation dynamics of the 5-state model, obtained from a numerically exact time propagation of the full product state wave-function. Apart from the states shown in (a), also the populations of the HOH bend fundamental ($|0,0,1\rangle$, green) and the ground state ($|0,0,0\rangle$, black) are depicted. The dotted line shows an exponential fit to the decay of $|1,0,0\rangle$. In panel (a) and (c), the insets focus into the very early time evolution.

converges to the same value at longer times, that is, the energy equipartitions. We find it remarkable that a small system with only six modes seems to thermalize on such a short time scale.

C. Calculation of spectra

1. Absorption spectrum

From the time-dependent wave-function $|\Psi(t)\rangle$, absorption spectra were calculated via

$$A(\omega) \propto \int_0^{T_{\max}} dt\, e^{-i\omega t} D(t)\, \langle \Psi(0)|\Psi(t)\rangle, \qquad (17)$$

where the Fourier transformation was extended up to $T_{\max}$ = 32.8 ps with time step 2 fs and apodized by the damping function $D(t)$. To reveal the details of the eigenstate structure of the spectrum, we used a Gaussian function for $D(t)$ resulting

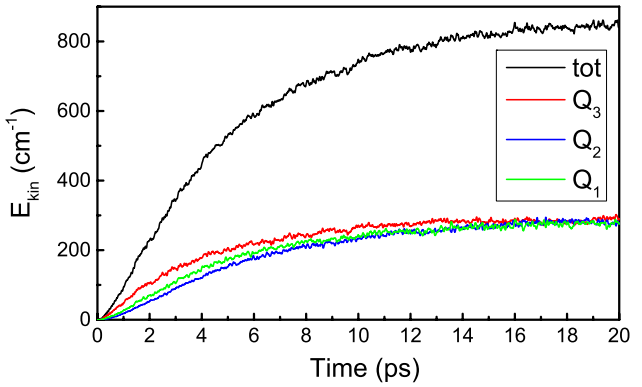

FIG. 6. Time evolution of kinetic energy of the low-frequency vibrations in the $|0,0,0\rangle$ ground state. The black curve shows the total kinetic energy, the green, blue, and red curves the kinetic energy subdivided into the three low frequency modes Q_1, Q_2, and Q_3, respectively.

in a spectral width of 1 cm^{-1} FWHM. Figure 7(a) shows the result obtained from a diabatic time-propagation in the absence of the coupling between the OH-stretch modes and the HOH-bend overtone. Below 3350 cm^{-1}, there is a single Franck-Condon progression with a spacing of 75 cm^{-1}; very close to the experimental value of 70 cm^{-1} (Fig. 8(c)).[26] It corresponds to a coherent wave-packet motion along Q_1 after excitation of the OH-stretch state. Above 3350 cm^{-1}, which roughly coincides with the curve crossing between the two OH-stretch PESs (Fig. 2, left panel), each Franck-Condon peak splits into two states. The spectrum of Fig. 7(a) is qualitatively the same as that of Ref. 18 for $CH_3NO_2^-\cdot H_2O$ and $CH_3CO_2^-\cdot H_2O$, or that of Ref. 22 for $NO_3^-\cdot H_2O$, both of which treated the problem on the level of a cubic expansion of the Born-Oppenheimer PES.

Turning on the coupling between the OH-stretch states $|1,0,0\rangle$ and $|0,1,0\rangle$ and the HOH-bend overtone $|0,0,2\rangle$, the resulting spectrum is shown in Fig. 7(b). Comparison to Fig. 7(a) tests the effect of that coupling for which we have seen that it causes significant transfer of population (Fig. 5(a)). We find that the effect of that Fermi resonance on the spectral response is in fact relatively small. In essence, some low-frequency states on the PES of the HOH-bend overtone mix in, which are marked by arrows in Fig. 7(b). That is, although the initial decay of the population into the HOH bend overtone through the conical intersection is ultrafast (60 fs) and irreversible (Fig. 5(a), inset), it does not result in significant line broadening. This is because the wave packet energy evolves energetically rather close to the bottom of the various PESs, where the density of states is still small and discrete.

Figure 7(c) shows the absorption spectrum obtained from the numerically exact time-propagation, which includes relaxation into the HOH-bend fundamental $|0,0,1\rangle$ as well as the ground state $|0,0,0\rangle$. Apart from a small frequency shift of 30 cm^{-1} (which we attribute to the fact that the set of diabatic states is not a complete basis, see Eq. (15)), the overall pattern of the spectrum is similar as in Fig. 7(b). Due to the nonadiabatic coupling of the initially excited vibrations to the lower states $|0,0,1\rangle$ and $|0,0,0\rangle$, however, we notice the onset of intensity-borrowing lines, some of which are partially resolved (in particular for the lowest frequency band), and others are not due to our limited spectral resolution of 1 cm^{-1}.

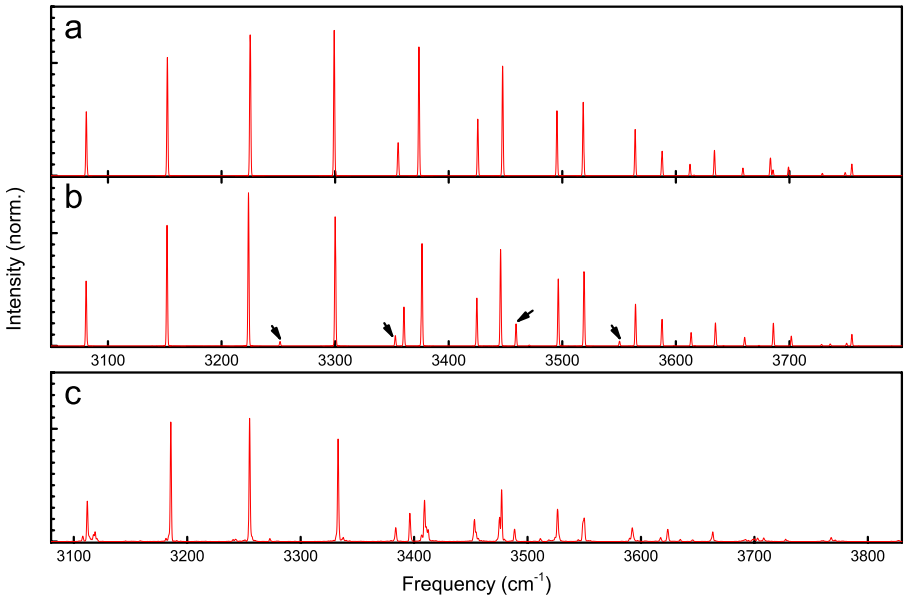

FIG. 7. Absorption spectrum after impulsive excitation of the symmetric OH-stretch vibration, (a) in a diabatic representation when switching off the coupling between the OH-stretch modes and the HOH-bend overtone, (b) in a diabatic representation in which that coupling is switched on, and (c) from the numerically exact time-propagation which includes also nonadiabatic couplings to the HOH-bend fundamental as well as the ground state (solid line). All three spectra are normalized to the same area.

As a consequence, various peaks appear to be a bit wider in terms of their FWHM and correspondingly lower in peak intensity (all spectra in Fig. 7 are normalized to the same area, and have been apodized by the same Gaussian function). Furthermore, the bands start to develop what looks like Lorentzian wings. The faster relaxation time (0.5 ps) extracted from the decay of the $|1,0,0\rangle$ state in Fig. 5 corresponds to a Lorentzian width of 10 cm^{-1} (FWHM), which is in reasonable agreement with the energy range within which intensity-borrowing substates are observed. Nonetheless, all three spectra in Fig. 7 appear quite similar, in contrast to the substantially different relaxation dynamics of the various models in Fig. 5, which might be more directly observed in a time-resolved experiment.

Each absorption band in the 3-state model (Fig. 7(b)) represents a single eigenstate of the corresponding Hamiltonian. Along the lines of Ref. 56, these states can be viewed as "zero-order bright" states that couple to a quasi-continuum of quasi-resonant dark states from the HOH bend fundamental $|0,0,1\rangle$ and the ground state $|0,0,0\rangle$ PESs, once the latter are added in the 5-state model. The energy width of coupled dark states around each zero-order bright state reflects the nonadiabatic coupling strength. The dark states that mix in are highly excited with respect to the low-frequency coordinates, as they originate from lower excitations with respect to the high frequency modes. As such, these dark states lie above the barriers separating the various hydrogen bonded isomers (see Fig. 4). The relevant Q-space is large and the density of states thus high, constituting a quasi-continuum of states. Furthermore, the HOH bend fundamental and ground state PESs are extremely anharmonic in this energy regime, thus randomizing the energy spectrum and rendering the relaxation process exponential.

2. Ar-tag spectrum

Johnson *et al.*[18,23–26] did not measure the absorption spectrum [Eq. (17)] directly, but an Ar-"tag" spectrum. In such an action spectrum, the absorbed light "heats" up the complex, leading to a dissociation of an Ar-atom that is very weakly bound to the complex, which in turn causes a change of mass of the complex that is eventually detected. Assuming that the Ar-atom dissociates from a fully thermalized complex, the Ar-"tag" spectrum reflects the total energy absorbed by the complex, and is therefore given by the IR absorption spectrum. However, it has been observed for similar complexes that the Ar atom typically dissociates on a 100 ps to 1 ns time scale,[57,58] and the assumption of full thermalization after such a short time is a bit questionable, given the small size of these complexes.

To model the Ar-tag spectrum in a more direct way, we therefore consider the kinetic energy content of the low-frequency modes, which account for the "heating" of the complex. Hence, we define the Ar-tag spectrum $I_{\mathrm{AT}}(\omega)$ as the expectation value of the kinetic energy T_Q after light absorption at long times as

$$I_{\mathrm{AT}}(\omega) = \lim_{t\to\infty} \langle \Psi_\omega(t)|T_Q|\Psi_\omega(t)\rangle, \tag{18}$$

where

$$\Psi_\omega(t) = \frac{i}{\hbar}\langle\psi_0^{\mathrm{dia}}| \int_0^t dt' e^{-i\omega t'} D(t') e^{-iH(t-t')/\hbar}|\Psi(0)\rangle \tag{19}$$

denotes the wave function obtained from time-dependent perturbation theory in first order. Here, the term $e^{-i\omega t'}$ describes the cw laser excitation of the system, while the propagator $e^{-iH(t-t')/\hbar}$ accounts for the nonadiabatic relaxation into the ground state $|0,0,0\rangle$, which in turn affects the heating of the molecule that is measured in the Ar-tag action spectrum. For computational convenience, we projected the total wavefunction on the diabatic ground state $|\psi_0^{\mathrm{dia}}\rangle$, which is expected to receive the highest amount of kinetic energy and hence will cause the largest effects. According to its definition in Eq. (19), the Ar-tag experiment is described as an excitation spectrum rather than by an absorption spectrum. For the practical computation of $I_{\mathrm{AT}}(\omega)$ via a Fourier transformation,

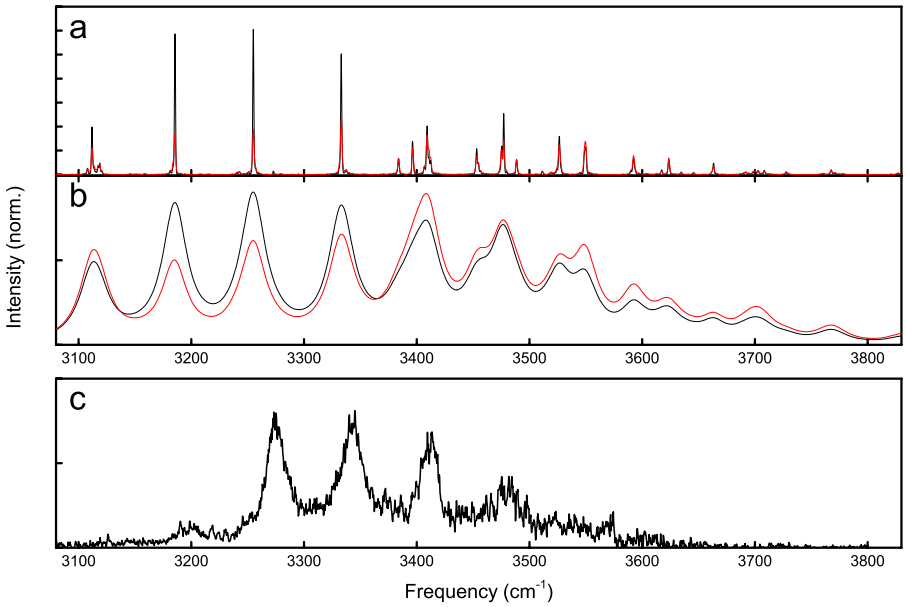

FIG. 8. Ar-tag spectrum [Eq. (20), red] and absorption spectrum [Eq. (17), black, same as in Fig. 7(c)], as obtained for the 5-state model of $HCO_2^-\cdot H_2O$. In panel (a), a Gaussian apodization function resulting in a spectral width of 1 cm^{-1} FWHM was employed, in (b), an exponential damping function with a decay time of $T_2 = 0.4$ ps, resulting in a Lorentzian lineshape with a spectral width of 25 cm^{-1} FWHM. In both cases, spectra are normalized to the same area. (c) Experimental spectrum taken from supplementary material of Ref. 26.

we rewrite Eq. (19) as

$$\Psi_\omega(Q) \propto \int_0^{T_{\max}} dt'\, e^{i\omega t'}\, D(T_{\max} - t')\, \langle \psi_0^{\mathrm{dia}} | \Psi(t') \rangle. \quad (20)$$

Figure 8(a) compares the resulting Ar-tag spectrum obtained for the 5-state model to the corresponding absorption spectrum, using again a Gaussian damping function that results in a spectral width of 1 cm^{-1} FWHM. The overall features of both spectra are quite similar, which might reflect the fact that energy indeed does reach an essentially thermalized state short after relaxation, as already seen by the equipartitioning of the kinetic energy (Fig. 6). In detail, the intensities of the individual substates vary somewhat, which is associated with the coupling of the corresponding state to the ground state, i.e., its capability to dump energy into low-frequency degrees of freedom. Overall speaking, higher frequency states get tentatively more intensity in the Ar-tag spectrum as compared to the absorption spectrum.

However, we find that neither the absorption spectrum nor the Ar-tag spectrum of the 5-state model in Fig. 8(a) reveal the broad background observed in the experiments of Johnson and coworkers (Fig. 8(c)).[26] To mimic the experimental spectral width, we may alternatively use an exponential damping function $D(t) = e^{-t/T_2}$ for both spectra, where $1/T_2 = 1/2T_1 + 1/T_2^*$ denotes the total dephasing rate that can consist of either pure dephasing T_2^* or additional relaxation channels T_1. Employing $T_2 = 0.4$ ps, the Lorentzian wings of the individual peaks merge to form a background (Fig. 8(b)) that qualitatively matches the experimental result (Fig. 8(c)).[26]

We can think of several reasons that could give rise to such an additional broadening. First, additional broadening can be caused by the remaining six vibrations of $HCO_2^-\cdot H_2O$ that are not included in the present model. These "spectator modes" may add additional weak line progressions, which might become a quasi-continuum when they are dense enough.[59] This possibility is supported by the observation that the broad background becomes more pronounced for complexes of water with larger molecules ($CH_3NO_2^-$ or $CH_3CO_2^-$),[23] in which case the complex consists of more degrees of freedom and at the same time is of lower symmetry. The effect of these additional vibrations could in principle be studied by using a simple model ansatz for the PESs and an advanced quantum-dynamical method such as MCTDH.[60] Second, one needs to keep in mind that the experimental system actually is not the isolated complex studied here, but contains a number of Ar-atoms needed for the Ar-tag spectroscopy. These Ar atoms are weakly bound through van der Waals interactions, i.e., modes of even lower frequency, that might constitute a "bath" that adds dephasing. In that regard, it is important to note that bands other than the OH stretch vibration, e.g., the CH stretch vibration of HCO_2^-, are significantly narrower. The larger width of the OH modes can be caused by their larger anharmonicity which makes them more susceptible to dephasing.[61] Finally, also the spectral resolution of the experimental setup may contribute to the total linewidth.

IV. CONCLUDING REMARKS

Based on extensive *ab initio* calculations, we have constructed a model of the vibrational dynamics of $HCO_2^-\cdot H_2O$ that comprises three high-frequency intramolecular vibrations and three low-frequency intermolecular vibrations of the complex (Fig. 1). To elucidate the involved relaxation dynamics following the excitation of the OH-stretch vibration, we have employed an adiabatic ansatz separating the two sets of modes. This results in a 5-state model that includes PESs of the ground state $|0,0,0\rangle$, the fundamentals $|0,0,1\rangle$, $|1,0,0\rangle$, and $|0,1,0\rangle$ of the HOH bend and the two OH stretch vibrations, and the first HOH bend overtone $|0,0,2\rangle$. To compare the simulation results to the experiments of Johnson *et al.*,[26] we calculated the spectral signatures of the vibrational dynamics on these PESs, both as absorption spectrum and as a mimic of an Ar-tag spectrum. In semiquantitative agreement with the experiment, these spectra are dominated by a single "Franck-Condon" progression of mode Q_1.

Studying the PESs of these states along the three low-frequency modes, we have identified a vibrational conical intersection seam between OH stretch states $|1,0,0\rangle$ and $|0,1,0\rangle$ and the closely resonant HOH bend state $|0,0,2\rangle$ (Figs. 2 and 3). The conical intersection affects an ultrafast (60 fs) and irreversible initial decay of the OH stretch population and gives rise to coherent wave packet motion on the coupled PESs (Fig. 5). In direct analogy to ultrafast photophysical or photochemical reactions in the electronic case, the adiabatic ansatz facilitates the interpretation of coherent population transfer processes through crossing PESs.[49,55]

On the other hand, when including the HOH bend fundamental $|0,0,1\rangle$ and the ground state $|0,0,0\rangle$ into the model, we find no curve crossings between these states and the energetically well separated excited states (Fig. 2). Population decay into these states occurs in an incoherent manner, that is, it hardly exhibits oscillations and is well described by exponential functions (Fig. 5). Hence, the mechanism of the subsequent population relaxation from the excited states into the lower-lying states in the 5-state model is distinctively different from the initial coherent population transfer in the 3-state model. The electronic analog of that relaxation mechanism is radiationless internal conversion in the weak coupling limit, which can be described in a perturbative manner, thus leading to a golden-rule-type description.[62] Considering, e.g., the $|1,0,0\rangle \rightarrow |0,0,1\rangle$ relaxation process, this means that a manifold of many highly excited vibrational states in the $|0,0,1\rangle$ state couple quasi-resonantly to comparatively few low-lying states in the $|1,0,0\rangle$ state.

In contrast to the electronic case, however, the time scale of the weak coupling relaxation $|1,0,0\rangle \rightarrow |0,0,1\rangle$ is only insignificantly slower than the curve crossing relaxation $|1,0,0\rangle \rightarrow |0,0,2\rangle$. In the electronic case, downhill relaxation through a conical intersection can be as fast as 10 fs,[63] while it is typically larger than the fluorescence lifetime (i.e., $\gtrsim$10 ns) when no curve crossings exist. In other words, the variability of electronic relaxation time scales exceeds six orders of magnitudes, while vibrational relaxation time scales cover only about one order of magnitude. This observation suggests that the adiabatic approximation may be relatively poor in the vibrational case, in the sense that essentially no decay should occur in the case of well-separated non-crossing adiabatic states if the approximation were good.

This finding seems surprising in the light of the fact that the separation of time scales between vibrational and electronic degrees of freedom (typically a factor of ten) is quite similar to the time scale separation between inter- and intramolecular degrees of freedom. It is that time scale separation which is often believed to be the condition for the adiabatic approximation to be good. However, a closer inspection of adiabatic Schrödinger equation (5) reveals that it is really the mass difference between light and heavy particles which counts, rather than the time scale separation *per se* (the time scale separation is only a consequence of the different masses). Adopting atomic units, all masses of a vibronic Hamiltonian are measured in units of the electron mass m_e. As a consequence, the kinetic energy of an electron is given by $-\frac{1}{2}\nabla_e^2$, while the kinetic energy of nuclei is given by $-\frac{1}{2M}\nabla_n^2$, where $M = m_n/m_e$ is nucleic mass in units of m_e. Since the nonadiabatic coupling operator Λ_{nm} in Eq. (5) can be written as[55]

$$\Lambda_{nm}(Q) = -\int dq\, \psi_n^{\mathrm{ad}}(q;Q)\left[T_Q, \psi_m^{\mathrm{ad}}(q;Q)\right] \propto M^{-1} = \frac{m_e}{m_n}, \tag{21}$$

the vibronic coupling is relatively small due to the factor m_e/m_n which is typically between 10^{-4} and 10^{-5}. In the vibrational case, on the other hand, the corresponding ratio $m_{\mathrm{HF}}/m_{\mathrm{LF}}$ between the masses of the high- and low-frequency modes is typically around 10^{-1}, that is, we expect in general larger nonadiabatic couplings even without any curve crossings.

The time scale of a particular degree of freedom scales as $\sqrt{m/k}$ (assuming a harmonic picture with k being the force constant), hence it is not only the mass ratio, but also the ratio in steepness of potentials that determines the time scale separation. In the electronic case with a mass ratio of 10^{-4} and to 10^{-5}, the potentials are such that they actually reduce the time scale separation from what would be expected from a simple $\sqrt{m}$ dependence. In contrast in the vibrational case, both the relatively small mass ratio and the potentials act in concert—intermolecular forces are weaker than intramolecular forces—to reveal about the same time scale separation as in the electronic case.

In conclusion, vibrational conical intersections, which have been shown to indeed exist for a variety of molecular systems (this work as well as in Refs. 28, 29, 37, and 38), present a less distinct pathway for energy relaxation as in the electronic case. Generally speaking, the interpretation of vibrational relaxation processes in terms of adiabatic PESs is therefore less straightforward than in the case of electronic relaxation. Nonetheless, the intuitive and appealing picture might be helpful, e.g., to study vibrational energy relaxation in liquids that involve a large number of quasi-resonant high-frequency modes.

ACKNOWLEDGMENTS

We are grateful to Mark Johnson for insightful discussions on the topic of the paper, as well as for making the experimental spectrum (Fig. 8(c)) available to us for a direct comparison. The work has been supported in part by the Swiss National Science Foundation (SNF) through the NCCR MUST.

[1]G. A. Jeffrey and W. Saenger, *Hydrogen Bonding in Biological Structures* (Springer, New York, 1991).
[2]G. D. Rose and R. Wolfenden, Annu. Rev. Biophys. Biomol. Struct. **22**, 381 (1993).
[3]P. G. Debenedetti, J. Phys.: Condens. Matter **15**, R1669 (2003).
[4]E. T. J. Nibbering and T. Elsaesser, Chem. Rev. **104**, 1887 (2004).
[5]H. J. Bakker and J. L. Skinner, Chem. Rev. **110**, 1498 (2010).
[6]D. Madsen, J. Stenger, J. Dreyer, E. J. Nibbering, P. Hamm, and T. Elsaesser, Chem. Phys. Lett. **341**, 56 (2001).
[7]J. Stenger, D. Madsen, J. Dreyer, E. T. J. Nibbering, P. Hamm, and T. Elsaesser, J. Chem. Phys. A **105**, 2929 (2001).
[8]D. Madsen, J. Stenger, J. Dreyer, P. Hamm, E. J. Nibbering, and T. Elsaesser, Bull. Chem. Soc. Jpn. **75**, 909 (2002).
[9]K. Heyne, N. Huse, E. T. J. Nibbering, and T. Elsaesser, Chem. Phys. Lett. **369**, 591 (2003).
[10]K. Heyne, N. Huse, J. Dreyer, E. T. J. Nibbering, and T. Elsaesser, J. Chem. Phys. **121**, 902 (2004).

[11]J. Edler, P. Hamm, and A. C. Scott, Phys. Rev. Lett. **88**, 067403 (2002).
[12]J. Edler and P. Hamm, Phys. Rev. B **69**, 214301 (2004).
[13]M. L. Cowan, B. D. Bruner, N. Huse, J. R. Dwyer, B. Chugh, E. T. J. Nibbering, T. Elsaesser, and R. J. D. Miller, Nature **434**, 199 (2005).
[14]K. Ramasesha, L. D. Marco, A. Mandal, and A. Tokmakoff, Nat. Chem. **5**, 935 (2013).
[15]F. Perakis, J. A. Borek, and P. Hamm, J. Chem. Phys. **139**, 014501 (2013).
[16]O. Henri-Rousseau and P. Blaise, Adv. Chem. Phys. **103**, 1 (1998).
[17]G. M. Florio, T. S. Zwier, E. M. Myshakin, K. D. Jordan, and E. L. Sibert, J. Chem. Phys. **118**, 1735 (2003).
[18]E. M. Myshakin, K. D. Jordan, E. L. Sibert III, and M. A. Johnson, J. Chem. Phys. **119**, 10138 (2003).
[19]J. Dreyer, J. Chem. Phys. **122**, 184306 (2005).
[20]K. Giese, M. Petkovic, H. Naundorf, and O. Kühn, Phys. Rep. **430**, 211 (2006).
[21]H. C. Liu, Y. M. Wang, and J. M. Bowman, J. Am. Chem. Soc. **136**, 5888 (2014).
[22]N. Heine, E. G. Kratz, R. Bergmann, D. P. Schofield, K. R. Asmis, K. D. Jordan, and A. B. McCoy, J. Phys. Chem. A **118**, 8188 (2014).
[23]W. H. Robertson, E. A. Price, J. M. Weber, J.-W. Shin, G. H. Weddle, and M. A. Johnson, J. Phys. Chem. A **107**, 6527 (2003).
[24]B. M. Elliott, R. A. Relph, J. R. Roscioli, J. C. Bopp, G. H. Gardenier, T. L. Guasco, and M. A. Johnson, J. Chem. Phys. **129**, 094303 (2008).
[25]R. A. Relph, B. M. Elliott, G. H. Weddle, M. A. Johnson, J. Ding, and K. D. Jordan, J. Phys. Chem. A **113**, 975 (2009).
[26]H. K. Gerardi, A. F. DeBlase, X. Su, K. D. Jordan, A. B. McCoy, and M. A. Johnson, J. Phys. Chem. Lett. **2**, 2437 (2011).
[27]D. J. Goebbert, E. Garand, T. Wende, R. Bergmann, G. Meijer, K. R. Asmis, and D. M. Neumark, J. Phys. Chem. A **113**, 7584 (2009).
[28]P. Hamm and G. Stock, Phys. Rev. Lett. **109**, 173201 (2012).
[29]P. Hamm and G. Stock, Mol. Phys. **111**, 2046 (2013).
[30]*Conical Intersections: Theory, Computation and Experiment*, edited by W. Domcke, D. R. Yarkony, and H. Köppel (World Scientific, Singapore, 2011).
[31]M. A. Robb, M. Garavelli, M. Olivucci, and F. Bernardi, Rev. Comput. Chem. **15**, 87 (2000).
[32]B. Levine and T. Martinez, Annu. Rev. Phys. Chem. **58**, 613 (2007).
[33]A. Staib and J. T. Hynes, Chem. Phys. Lett. **204**, 197 (1993).
[34]A. Staib, D. Borgis, and J. T. Hynes, J. Chem. Phys. **102**, 2487 (1995).
[35]G. L. Barnes, S. M. Squires, and E. L. Sibert, J. Phys. Chem. B **112**, 595 (2008).
[36]G. Hanna and E. Geva, J. Phys. Chem. B **115**, 5191 (2011).
[37]M. B. Dawadi and D. S. Perry, J. Chem. Phys. **140**, 161101 (2014).
[38]B. P. Thapaliya, M. B. Dawadi, C. Ziegler, and D. S. Perry, Chem. Phys. (2015).
[39]M. J. Frisch, G. W. Trucks, H. B. Schlegel, G. E. Scuseria, M. A. Robb, J. R. Cheeseman, G. Scalmani, V. Barone, B. Mennucci, G. A. Petersson *et al.*, GAUSSIAN *09 Revision A.1*, Gaussian, Inc., Wallingford, CT, 2009.
[40]X.-G. Wang and T. Carrington, J. Chem. Phys. A **105**, 2575 (2001).
[41]D. T. Colbert and W. H. Miller, J. Chem. Phys. **96**, 1982 (1992).
[42]Q_2 represents a linear translation with a kinetic energy operator $T_Q \propto \partial^2/\partial Q_2^2$, whose DVR representation is given by Eq. (A6) of Ref. 41. On the other hand, Q_1 and Q_3 are linear combinations of rotations of the two molecules (Fig. 1). Since we consider only 1D rotations due to restricting the problem to modes that stay in the plane of the complex, the corresponding kinetic energy operator remains simple with $\propto \partial^2/\partial\alpha_i^2$ (where α_i are the rotation angles of the two molecules). In principle, a DVR exists for that operator that takes its periodicity into account.[41] Since we, however, combine two angles with different scaling factors into one mode (so that their linearisations for small displacements reveal the corresponding normal mode coordinates), the overall coordinates Q_1 and Q_3 are no longer periodic. We therefore use Eq. (A6) of Ref. 41 for the angle coordinates as well. Since the maximum rotation in the considered region is still significantly smaller than 2π, that approximation appears to be acceptable.
[43]P. Jungwirth and R. B. Gerber, Chem. Rev. **99**, 1583 (1999).
[44]J. O. Jung and R. B. Gerber, J. Chem. Phys. **105**, 10332 (1996).
[45]Apart from convergence issues, it is in fact irrelevant for both the adiabatic and the diabatic representation whether or not the minimum energy positions $\{q_i^{(0)}\}$ in Eq. (10) are considered (discarding them actually leads to slightly better convergence with respect to basis size). On the other hand, for the numerically exact time-propagation, it is mandatory to expand Eq. (10) and to consider the minimum energy positions explicitly. We have found that it is the variation of the minimum energy positions $\{q_i^{(0)}\}$ as a function of inter-molecular coordinates Q that dominates the non-adiabtic couplings between the excited states to the bend fundamental and the ground state.
[46]H. Tal-Etzer and R. Kosloff, J. Chem. Phys. **81**, 3967 (1984).
[47]H. Köppel, W. Domcke, and L. S. Cederbaum, Adv. Chem. Phys. **57**, 59 (1984).
[48]W. H. Press, S. A. Teukolsky, W. T. Vetterling, and B. P. Flannery, *Numerical Recipes in C* (Cambridge University Press, Cambridge, 1992).
[49]A. H. Zewail, J. Phys. Chem. A **104**, 5660 (2000).
[50]J. C. Deàk, S. T. Rhea, L. K. Iwaki, and D. D. Dlott, J. Phys. Chem. A **104**, 4866 (2000).
[51]S. Ashihara, N. Huse, A. Espagne, E. Nibbering, and T. Elsaesser, Chem. Phys. Lett. **424**, 66 (2006).
[52]A. M. Dokter and H. J. Bakker, J. Chem. Phys. **128**, 024502 (2008).
[53]L. De Marco, K. Ramasesha, and A. Tokmakoff, J. Phys. Chem. B **117**, 15319 (2013).
[54]G. Stock, R. Schneider, and W. Domcke, J. Chem. Phys. **90**, 7184 (1989).
[55]W. Domcke and G. Stock, Adv. Chem. Phys. **100**, 1 (1997).
[56]D. J. Nesbitt and R. W. Field, J. Phys. Chem. **100**, 12735 (1996).
[57]J. D. Pitts and J. L. Knee, J. Chem. Phys. **109**, 7113 (1998).
[58]J. D. Pitts and J. L. Knee, J. Chem. Phys. **110**, 3389 (1999).
[59]G. Stock, J. Chem. Phys. **101**, 246 (1994).
[60]*Multidimensional Quantum Dynamics*, edited by H. D. Meyer, F. Gatti, and G. A. Worth (Willey-VCH, Weinheim, 2009).
[61]J. Stenger, D. Madsen, P. Hamm, E. T. J. Nibbering, and T. Elsaesser, Phys. Rev. Lett. **87**, 027401 (2001).
[62]R. Englman and J. Jortner, Mol. Phys. **16**, 145 (1970).
[63]Y.-I. Suzuki, T. Fuji, T. Horio, and T. Suzuki, J. Chem. Phys. **132**, 174302 (2010).